Lab-on-a-Fiber Device for Trace Vapor TNT Explosive Detection: Comprehensive Performance Evaluation

Jianjun Ma, Aldona Kos, Wojtek J. Bock, *Fellow, IEEE*, Xianzhe Li, Huy Nguyen, Zhi Yuan Wang, and Andrea Cusano

***Abstract*—Based on the previously proposed concept of a lab on a fiber (LOF) and an LOF-based platform for detecting trace vapors of TNT explosives, in this paper, we study the compatibility of the LOF device with a preconcentration unit. We report the detail investigation of factors that crucially affect the overall performance of this LOF platform. From a theoretical perspective, we investigate the efficiency of a light source formed at the fiber tip on sensory film excitation. Experimentally, we demonstrate the much faster response time of the LOF over a sensory film on a bulky planar glass substrate. We also evaluate the following factors that significantly impact the sensitivity of the instrumentation system: 1) the proper bond between the sensory film and the fiber surface; 2) the concentration of polymer solution for thin-film formation; and 3) the degradation of thin film in the presence of ambient light and the oxygen content in the air.**

***Index Terms*—Explosions, explosives, gas detectors, national security, optical fiber sensors, polymer films, thin-film sensors.**

I. Introduction

In our previous work, we introduced the concept of a lab on a fiber (LOF), a fiber-optic sensing platform that includes standard laboratory functions downsized to the millimeter scale [1]. This concept was further developed through the illustration of an LOF device for trace vapor TNT detection with the emphasis on choosing the proper combination of components among available fiber-optic sensor (FOS) designs [2]. The preliminary theoretical work on the performance of the proposed two-fiber side-by-side LOF device based on evanescent wave (EW) [2] was presented in [3]. The structure of the LOF is such that one or more fibers within this small device serve not just as a traditional means of transmitting an excitation light (e-light) and/or a signal light (s-light). Nor does the LOF simply fall into the category of the intrinsic FOS or the all-fiber sensor that is able to sense and transmit signals simultaneously. Rather, the fibers in an LOF device are substrates that are integrated with optical elements such as a light-source shaper, a mirror, a lens, an optical signal collector, and an enhancer. These components are directly built on the fiber in various forms depending on the applications, or they are created by shaping fiber itself. This not only ensures the tiny size of the LOF device but also maximizes its robustness, another major goal for the LOF proposition. Functions associated with chemical processes might also be included by attaching them directly to the fiber via proper techniques.

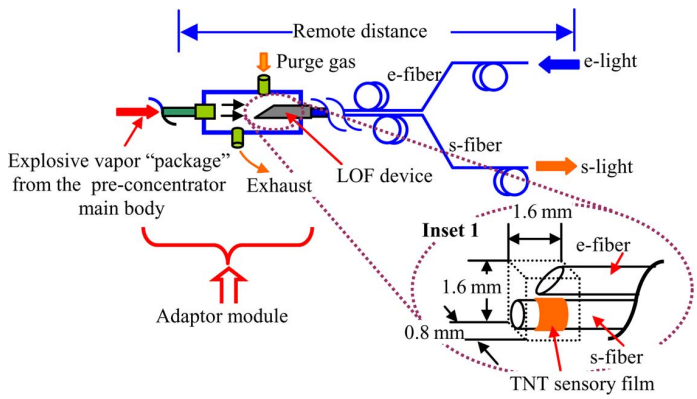

Fig. 1. Example showing an LOF device in the adaptor module. Its tiny internal space ensures high concentration of the sample received from the preconcentrator main body. The received sample "package" is also sent to the LOF sensing area as a "package." Inset 1 illustrates the architecture and the size of the LOF device. Legend: e-fiber: excitation fiber; s-fiber: signal fiber.

Among the excellent applications of an LOF architecture is the identification of the presence of explosives in critical infrastructures such as airports, railway stations, subways, commercial centers, and government buildings. The advantages of an LOF platform are not limited to its robustness, portability, or stealth sensing and remote monitoring capability. It also offers the best compatibility with the explosive vapor preconcentrator, a critical unit in the instrumentation system to minimize the probability of both missed detection and false alarms. The connection between the detector and the preconcentrator main body, however, has its specific requirements. Fig. 1 shows an adaptor module to properly establish the connection between our LOF device, which has the remote monitoring capability, and the preconcentrator main body. This adaptor module has a

Manuscript received July 08, 2011; revised September 22, 2011; accepted September 22, 2011. Date of publication September 29, 2011; date of current version March 09, 2012. This work was supported in part by the Natural Sciences and Engineering Research Council of Canada, the Canada Research Chairs Programme, the Ministère de Développement économique, Innovation et Exportation du Québec, and NATO Linkage Grant.

J. Ma, A. Kos, and W. J. Bock are with the Département d'informatique et d'ingénierie, Centre de recherche en photonique, Université du Québec en Outaouais, Gatineau, QC J8X 3X7, Canada (e-mail: ma.jianjun@uqo.ca; aldona@if.pw.edu.pl; wojtek.bock@uqo.ca).

X. Li, H. Nguyen, and Z. Y. Wang are with the Department of Chemistry, Carleton University, Ottawa, ON K1S 5B6, Canada (e-mail: xianzhen_li@carleton.ca; huy0320@gmail.com; wayne_wang@carleton.ca).

A. Cusano is with the Department of Engineering, Optoelectronics Division, University of Sannio, Benevento 82100, Italy (e-mail: a.cusano@unisannio.it).

Color versions of one or more of the figures in this paper are available online at http://ieeexplore.ieee.org.

Digital Object Identifier 10.1109/JLT.2011.2170154

small internal chamber and contains the following fundamental elements: 1) an inlet for concentrated explosive vapor; 2) an inlet to bring in purge gas to clean the detector surface after measurement; and 3) an outlet to get rid of the waste. The design of this module must take into consideration the concentration of the sample, which is the trace explosive vapor from the open air in our discussion. In this case, a parts-per-trillion level concentration is so common that not only is a preconcentrator mandatory, but a tiny space is needed to contain the detector within the adaptor module, or the LOF device in our case, in order to maintain the highest possible concentration to ensure a good reading. This is especially true when the total number of collected explosive particles is extremely sparse. To cope with this worst case scenario, the first priority in the design phase is to have the smallest possible detector, making the LOF device an excellent choice.

Inset 1 of Fig. 1 illustrates the proposed LOF device [1]–[3] with a size that fits into a 1.6 mm $\times$ 1.6 mm $\times$ 0.8 mm, fulfilling the requirements of the aforementioned adaptor module. Two identical fibers (BFL37-800 from Thorlabs, Inc., Newton, NJ) with core diameter, cladding diameter, and NA of 800, 830 μm, and 0.37, respectively, are used for excitation light delivery (e-fiber) and signal light collection (s-fiber). Within this cube, the e-fiber has a slanted end face to directly serve as a mirror that partially reflects the coming excitation light to the sidewall of the adjacent fiber where a short section of the TNT sensory film is coated. The film is specifically synthesized to respond to the presence of TNT vapor based on the mechanism of fluorescent quenching [4].

Despite its potential significance and many advantages, an LOF device for sensing purposes requires careful study. One of the greatest concerns we might have in a real-life situation is that it permits the sensing section no longer than a few millimeters, which in this case is approximately 0.8 mm (see Inset 1 of Fig. 1). This requirement poses challenges in every aspect of the system. In terms of the sensory material, it may affect the quantum efficiency of the sensory film, the quenching percentage after exposure to low vapor pressure. From the perspective of optics, it may compromise the efficient use of the excitation light for film excitation, i.e., the ability to achieve the highest possible fluorescent power level with no photon degradation effect. Techniques lying in between involve the uniform formation of the film on the fiber surface and creation of the thinnest possible film while maintaining resolvable quenched power limited by the nonquenching-related fluorescent power fluctuation and the performance of the detector.

In this paper, for the LOF device in Inset 1 of Fig. 1, we investigate the efficiency of coupling of the excitation light from the e-fiber to the sensory film on the sidewall of the s-fiber with the emphasis on an adjustable overall sensing length. The critical factors affecting the aforementioned overall instrumentation system performance are evaluated by combining this LOF device with sensory film and exposing it to simulated TNT explosive vapor. Other factors such as the lifetime of the synthesized polymer under regular storage conditions and film degradation due to ambient light exposure are experimentally investigated as well.

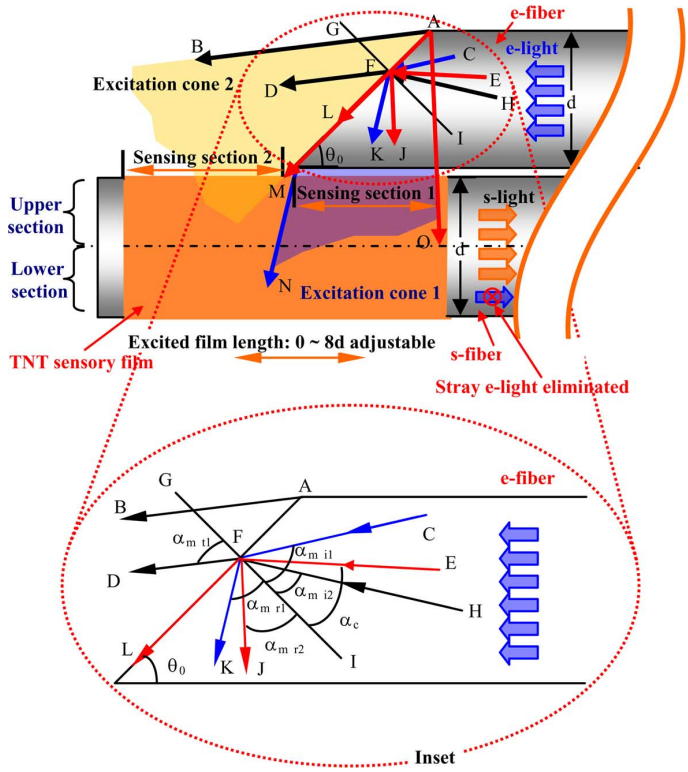

Fig. 2. Theoretical illustration of highly efficient thin-film sample excitation and s-light collection of the proposed LOF device. Adjustable sensing length from 0 to $8d$ is enabled by sliding either the e- or the s-fiber. Inset: detailed ray tracing to calculate the effective power for sample excitation after departing from the e-fiber core. Note that in principle, the e-fiber delivers the s-light with no stray e-light component.

II. Theoretical Investigation

A. Thin-Film Excitation With an Intensity Adjustable Light Beam

In a traditional EW-based fiber-optic sensing platform, the excitation light is fed from the end face of the fiber, leading to the weak EW signal power due to the fact that the excitation power is also in EW form [5], [6]. The thin film in our LOF design is excited via refracting and reflecting processes (see Inset of Fig. 1). This not only enables much more efficient use of the excitation power, but also concentrates this power on a very short fiber segment. Moreover, the tilted end face shapes the incoming circular light spot into a narrow excitation-light beam profile without demanding additional optical or mechanical components, an arrangement that specifically suits the thin-film sample distributed along the s-fiber and minimizes the size of the LOF device.

A further examination of this sensing architecture reveals more features offered by this tilted end face. The optical ray tracing, shown in Fig. 2, indicates that the refraction and reflecting processes create two excitation cones: 1) excitation cone 1 that is filled with light via reflection; and 2) excitation cone 2 that is occupied by light received through refraction. Although the launching cone of the e-fiber disperses the light power into free space, the overall power density at the s-fiber core–cladding surface remains high due to the tiny distance between the two fibers. For the end face with a tilted angle of

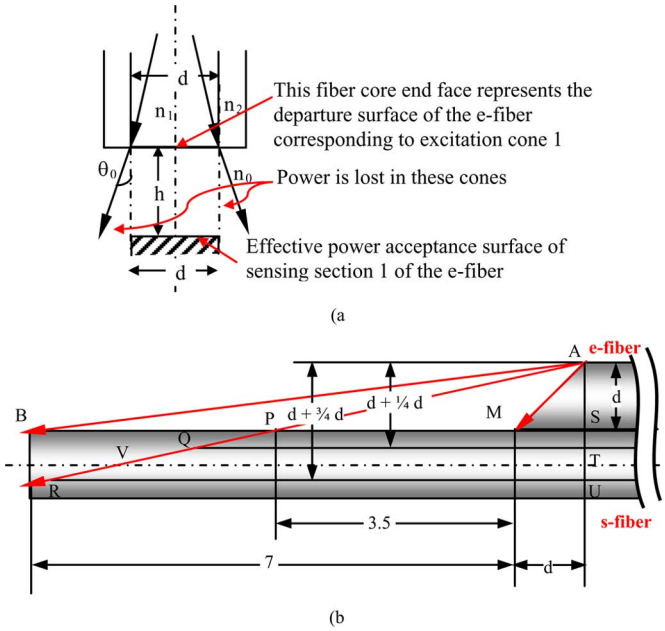

Fig. 3. Theoretical models to calculate the effective excitation power received by sensing sections 1 and 2. (a) Model for both sensing sections for calculating the effective power. (b) Model specifically for sensing section 2. The midpoint P is used to determine the average effective excitation power in this section.

$\theta_0 = 45°$ and core/cladding refractive indexes of 1.48/1.44, for example, the ray tracing shows that excitation cone 1 not only includes most of the excitation power, but also possesses much higher power density in comparison with excitation cone 2, which is discussed in the following.

B. Effective Excitation Power Within the Excitation Cone 1

Referring to rays at incident point F in Fig. 2, excitation cone 1 receives the incident light rays within the range of 15° from $\alpha_c = 43°$ to $\alpha_{m\_i1} = 58°$, determined by rays CF and EF. The rays propagating along and near the fiber axis that usually carry stronger light power are also included in this range. Referring to rays FK and FJ but keeping in mind that they are in fact enclosed by rays MN and AO, we see that the reflected power is concentrated within the same range as the incident light, which is also 15°. Obviously, the illuminated length of the s-fiber, when tight against e-fiber, is approximately the core diameter of the e-fiber ($1d$). As a simple and conservative estimate, we use the distance between the e-fiber exit at its core sidewall surface and the s-fiber axis, which is $0.5d$ when s- and e-fiber cores are tight together, as the separation between the two fibers when calculating the average power received by the two sensing sections. Excitation cone 1 includes at least half of the overall coming power P_0 and thus

$$P_{\text{cone1}} > 0.5P_0. \tag{1}$$

The separation $0.5d$ causes P_{cone1} to spread either in the fiber core or free space. Only the power remaining on the core surface participates the sample excitation. After distance $0.5d$, part of the excitation power received by sensing section 1 is lost in free space, the amount being determined by the numerical aperture of the e-fiber, which is $\text{NA} = n_0 \sin\theta_0$ as shown in Fig. 3(a). In the case of the simplified model in Fig. 3(a), the effective power for sample excitation in sensing section 1 is expressed by

$$P_{e1} > P_{\text{cone1}} \times \left[\frac{d}{2 \times h \times \text{NA} + d}\right]^2 = P_{\text{cone1}} \times d^2 \times \left[\frac{1}{2 \times \frac{h}{d} \times \text{NA} + 1}\right]^2 \tag{2}$$

where h represents the distance between the e-fiber exit surface and the surface of the s-fiber receiving the effective excitation power. It is assumed here that $tg\theta_0 \approx \sin\theta_0 = \text{NA}$.

The use of ">" in (2) arises from the implied assumption that the excitation power is uniformly distributed across the fiber core cross section. In reality, most of the power is confined within the central area of the fiber core, and thus, the power P_{e1} is much higher than the estimated value from the right-hand side of (2). Another ignored positive effect is that the excitation light rays have to pass the curved surface of sidewall of the e-fiber before entering free space. This curved surface acts as a focusing lens, tending to bend rays toward each other and, thus, reducing the light-spread effect, especially when the two fibers are tight against each other. Bearing these points in mind, we have to recognize that the estimates given here are too pessimistic. As an example, for the fiber with $\text{NA} = 0.37$, $h = 0.5d$, and $d = 0.8$ mm, (2) yields

$$P_{e1} > 34\%P_{\text{cone1}} \gg 17\%P_0. \tag{3}$$

However, we expect that the use of the excitation power to be considerably better than this.

C. Effective Excitation Power Within the Excitation Cone 2

Regarding excitation cone 2, the incident light rays that eventually arrive at this cone fall within the angle range from $\alpha_{m\_i2} = 32°$ to $\alpha_c = 43°$, enclosed by rays HF and EF. With a range of only 11° and given the lack of rays from the fiber axis and its neighborhood, the overall power entering the excitation cone 2 will be much less than would be expected from excitation cone 1. Excitation cone 2 is framed by rays AB at $\alpha_{m\_t1} = 52°$ and the tilted surface of the e-fiber. It is evident that this cone can be as wide as 38°, and that a large number of rays have to travel a long distance before reaching the s-fiber surface, especially those rays near the angle of $\alpha_{m\_t1} = 52°$. As a result, the power will be spread along a segment of s-fiber that can be as long as $7d$—see sensing section 2 in Fig. 3(b). The power density in sensing section 2 monotonously decreases from point M toward the end face of the s-fiber. All the aforementioned factors indicate that when compared to the power densities at the e-fiber surface where the thin-film resides, the average power density at the e-fiber surface covered by excitation cone 1 will be much larger than that at the s-fiber surface covered by the excitation cone 2.

As in the case of excitation cone 1, the overall power entering excitation cone 2 is

$$P_{\text{cone2}} < 0.5P_0. \tag{4}$$

Similarly, the effective excitation power in sensing section 2 can be estimated using the model shown in Fig. 3(a), with the

separation between fibers replaced by the average distance between the tilted end face and sensing section 2. The calculation of this distance, however, has to refer to the distance AV illustrated in Fig. 3(b), where V is a point at the s-fiber axis. The simple geometry determines that $\mathrm{AV} = 5.6d$. Then (2) becomes

$$P_{e2} > P_{\mathrm{cone2}} \times d^2 \times \left(\frac{1}{11.2\mathrm{NA}+1}\right)^2. \quad (5)$$

For the same fiber parameters used for (3), the estimated effective excitation power at sensing section 2 is

$$P_{e2} > 2.4\% P_{\mathrm{cone2}}. \quad (6)$$

Again, this is a very conservative estimate. In Fig. 1(b), for the same reason, a large number of rays close to the ray AB carry only small percentage of the overall power. Most of the refracted power, falling into excitation cone 2, is concentrated in the region near the ray AM where the separation between the e- and s-fibers is also close to $0.5d$. The more optimistic estimate is thus

$$P_{\mathrm{cone2}} \times d^2 \times \left(\frac{1}{\mathrm{NA}+1}\right)^2 > P_{e2} > P_{\mathrm{cone2}} \times d^2 \times \left(\frac{1}{11.2\mathrm{NA}+1}\right)^2. \quad (7)$$

Equation (6) is, thus, modified to be

$$34\% P_{\mathrm{cone2}} > P_{e2} > 2.4\% P_{\mathrm{cone2}} \text{ or } 17\% P_0 > P_{e2} > 1.2\% P_0. \quad (8)$$

D. Further Examination of the Effective Excitation Power by Considering Upper and Lower Sensing Sections

When further examining all conditions assumed to obtain (2) and (7) and thus (3) and (8), we realize that these equations are the result of average excitation power from both the upper sensing sections, which have a distance of 0 from the e-fiber, and the lower sensing sections, which have a distance of d from the e-fiber. Due to the curved shape of both upper and lower sensing sections, a further meaningful assumption is to calculate the average effective excitation power in both upper and lower sections. With the distance replaced by $1/4d$ and $3/4d$, respectively, the effective excitation power values for the upper and lower sections of sensing section 1 are, from (2)

$$P_{e1\_\mathrm{Upper}} > 46\% P_{\mathrm{cone1}} > 23\% P_0 \quad (9)$$

$$P_{e1\_\mathrm{Lower}} > 26\% P_{\mathrm{cone1}} > 13\% P_0. \quad (10)$$

The determination of the distance of the upper and lower sensing sections for sensing section 2 is illustrated in Fig. 3(b).

The midpoint P of sensing section 2 is adopted to estimate the average effective excitation power received by sensing section 2 of the s-fiber, which is $3.5d$ in length. We chose the plane QT perpendicular to this paper and at the position $d + 1/4d$ to intercept the s-fiber and obtain a cross section to represent the effective surface for the upper sensing section. Likewise, the effective surface for the lower sensing section is determined by the plane RU at $d + 3/3d$. The distances AQ and AR are $4.65d$ and $6.48d$, respectively, following the simple geometrical relationship. With these two factors, the effective excitation power received by each of the two sensing sections is derived from (2)

$$P_{e2\_\mathrm{upper}} > P_{\mathrm{cone2}} \times d^2 \left[\frac{1}{2 \times (4.65) \times \mathrm{NA}+1}\right]^2 = 3.2\% P_{\mathrm{cone2}} = 1.6\% P_0 \quad (11)$$

and

$$P_{e2\_\mathrm{lower}} > P_{\mathrm{cone2}} \times d^2 \left[\frac{1}{2 \times (6.48) \times \mathrm{NA}+1}\right]^2 = 1\% P_{\mathrm{core}} = 0.5\% P_0. \quad (12)$$

The maximized effective excitation power in sensing section 2 occurs at point M in Fig. 3(b). The distance between A and the center of the s-fiber is found to be $2.12d$, which leads to $P_{e2} > 9.6\% P_{\mathrm{cone2}} = 4.8\% P_0$. If we compare this figure with 17% of (3), we see that it is still fourfold less than the average effective excitation power in sensing section 1.

From (3), (9), (10) with (8), (11), (12) and considering the fact that $P_{\mathrm{cone1}} > P_{\mathrm{cone2}}$, a conservative conclusion is that sensing section 1 uses excitation power at least one order of magnitude more efficient than sensing section 2. The upper part of both sensing sections uses excitation power more efficiently than the lower part, approximately two to three times more efficiently. All these figures vary significantly depending on the square of the fiber core diameter as shown in (5), indicating the significance of using large-core fiber as both e- and s-fibers. Obviously, the overall EW signal will be dominated by sensing section 1 with a length of just $1d$, and the contribution from sensing section 2 can in fact be ignored.

E. Adjustable Sensing Length and Excitation Power Density

In Fig. 3, by sliding e- or s-fiber along its fiber axis, we can adjust the length of the overall sensing section—the combination of sensing sections 1 and 2—from virtually 0 to $8d$, depending on the desired signal level or sensing length. For fiber with an 800 μm core, this allows the sensing length to switch between 0 and 6.4 mm. Again, it is expected that the EW fluorescent signal from the thin film in sensing section 1, with merely $1d$ in length or 0.8 mm for an 800-μm-core fiber, will dominate the detectable power at the receiving end of the s-fiber.

In addition, the architecture in Fig. 3 makes it simpler to achieve adjustable power densities in both sensing sections. If we consider the architecture proposed in [7] and [8] with the e- and s-fibers perpendicular to each other, nearly all excitation power is forced to form a spot as tiny as the fiber core to excite the liquid sample droplet. One possible scenario with this design is the creation of an extremely high power density, triggering sample degradation or permanent damage to the sample. A wider gap between the two fibers might reduce this effect, but at the cost of losing a large amount of excitation power and, thus, affecting the overall collectable fluorescent emission power. In contrast, the arrangement of the two fibers and the tilted surface in Fig. 1(b) adjusts the excitation power density to approximately half the level in sensing section 1 but to a significantly lower level in sensing section 2 without sacrificing the overall power. From an engineering point of view, this arrangement greatly simplifies the packaging process, making the

overall sensing area more rugged, elegant, and cost-effective. In another extreme scenario, when samples demand more focused excitation power, a reflective coating on the tilted surface can switch virtually all incoming excitation power to sensing section 1, producing a spot size about the same diameter as the fiber core.

III. Experimental Investigation

A. Regarding the TNT Explosive Sensory Polymers

Two series of fluorescence "turn-off" polymers, represented by PL 4a, 4b and 5a, 5b, were synthesized for the detection of nitroaromatic compounds (NACs) such as 2,4,6-trinitrotoluene (TNT) [4]. These polymers are made by the Suzuki cross-coupling reaction of dibromide and bisboronic acid ester monomers. For polymers 4a and 4b, the monomer is designed to have an electron-donating diphenylamine moiety, in order to probe any donor–acceptor interaction with the electron-accepting NACs, thus, enhancing the detection sensitivity. Polymers 5a and 5b are synthesized by grouping the bulky cholesterol esters and long alkyl chains with the chosen monomers, which creates a site-isolating group to prevent the interchain interaction and form a large free volume in the resulting polymers. Such polymers enhance fluorescence quantum efficiency and help to trap analyte molecules.

B. Proper Formation of Film on the Fiber Sidewall

The film on the sidewall of the s-fiber was deposited via dipping. To ensure the uniform formation of the film, a proper pretreatment of the substrate with another specific chemical material, or adhesion promoter, is required to assist in bridging or establishing a chemical bond between the organic polymer and the inorganic substrate. Among available adhesion promoters, organofunctional silanes are excellent candidates. They are used as adhesives or sealant materials since they afford good adhesion, good mechanical properties, and also storage stability. In our fiber probe preparation process, we chose 3-aminopropyltrimethoxysilane, $H_2N(CH_2)_3Si(OCH_3)_3$, as the adhesion promoter. Purchased from Fluka, it has a concentration of 97%. The dipping process follows the sequence of promoter, water, and TNT sensory polymer solution. Dipping into water is an important step in that it provides the moisture needed for the silane's alkoxy groups to hydrolyze and react with the inorganic substrate, forming a bond covalently to the inorganic substrate such as the fiber core.

C. Quenching Response of Film on LOF versus on Planar Substrate

A series of experiments was performed to compare the quenching responses of this LOF device with those of a film coated on a planar glass substrate, the latter being a popular means adopted for sample performance evaluation in the lab. The advantages of the film on a bulky glass substrate lie in the fact that both the thickness and flatness of the film can be precisely controlled and measured by the use of a spin coater and many readily available instruments such as an ellipsometer or various types of profilers.

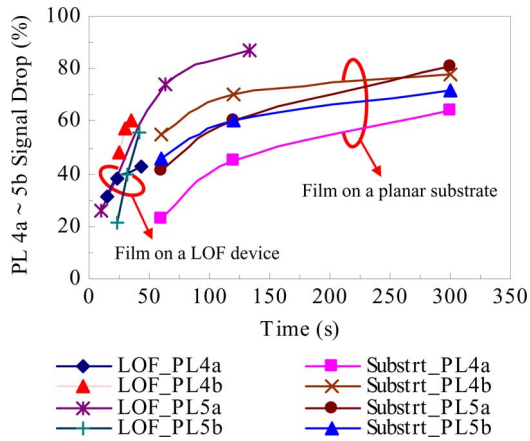

Fig. 4. Experimental results of TNT sensory film fluorescent quenching for devices based on an LOF and a planar substrate. Curves include the results from all four polymers PL 4a, 4b, 5a, and 5b. It is evident that the LOF device has a much faster response than the planar substrate device.

The polymer solution (5.0 mg in 1.0 mL of chloroform) was spin-coated onto a glass substrate with a size of 23 mm × 23 mm × 1 mm at a spin rate of 1000 r/min using the Chemat Technology spin-coater KW-4B. The film thickness was 65 nm, as measured using a Tencor Alpha-Step 200 surface profiler. The polymer films on optic-fiber tips were dip-coated in chloroform solution (1.5 mg/mL) and air-dried. The film thickness was measured by AFM to be 90 nm.

The TNT explosive vapor is simulated by its well-known precursor, 2,4-dinitrotoluene (DNT). The DNT powder is sealed in a bottle measuring $\phi 45 \times 50$ mm, helping to promptly reach the stabilized DNT vapor pressure. For the LOF device, the quenching effect can be easily monitored and recorded continuously by keeping one end of the fiber bundle containing the tiny LOF device inside the bottle via a small $\phi 10$ opening (similar to the case in Fig. 1). At the other end of the fiber bundle outside the bottle, the e-fiber leg is connected to an LED with its central wavelength at 375 nm. The s-fiber leg is connected to a hand-held spectrometer (USB 2000 from Ocean Optics, Dunedin, FL). For the bulky planar substrate, however, one has to monitor the fluorescent quenching by recording fluorescence spectra following two steps. First, the film-coated substrate is immersed in the bottle containing the DNT for a specific period of time. Second, it is removed from the bottle and immediately inserted into the lab-based analytical-level spectrometer for spectrum recording. By repeating the two steps, the quenching percentages versus different exposure times are obtained.

The experimental results for the fluorescent signal drop versus exposure time exhibited by polymer sensory film coated on the LOF and the planar substrate are plotted in Fig. 4. Results for all four polymer materials PL 4a, 4b, 5a, and 5b are included. For a planar substrate, the first 50 s is inaccessible since it is the setup time to manually transfer the sample substrate from the DNT exposure site to the lab-based spectrometer before data acquisition. Notwithstanding such a setup time, the trends of curves in Fig. 4 clearly show that for all four materials, the LOF device demonstrated far superior performance in responding to the presence of the DNT vapor. For example,

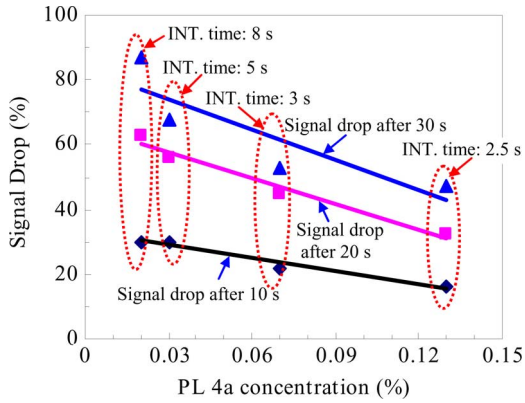

Fig. 5. Fluorescent quenching responses of the LOF to DNT vapor with different thin film thicknesses adjusted by dipping into the polymer solutions with the following concentrations: 0.02%, 0.03%, 0.07% and 0.13% with chloroform as the solvent. INT. time: integration time.

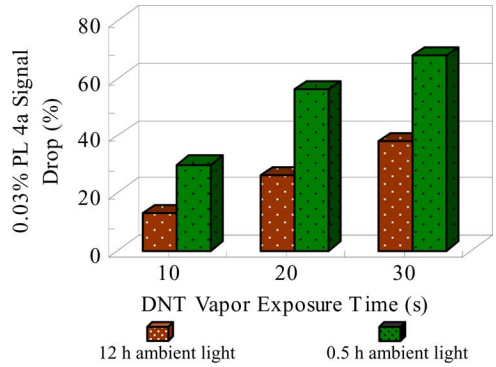

Fig. 6. Ambient light effect on the fluorescent quenching percentage for film formed by 0.03% PL 4a polymer concentration. It is evident that a lengthy exposure to ambient light degrades the polymer film and greatly slows down the quenching response.

curves associated with the LOF device show that for all four polymer films, over 35% of the fluorescent signal drop occurs in the first 40 s. These curves are also far steeper than those associated with the planar substrate, indicating the much higher sensitivity of the LOF device. When comparing the quenching effect of the two devices based on the same polymer film, the higher performance of the LOF device is even more evident. We attribute this fast response to the tiny size of the LOF device, whose active film area is a mere 2 mm^2 for an 800 μm fiber with a film length of 0.8 mm along the fiber.

D. Effect of Polymer Concentrations on the Quenching Performance of the LOF Device

The thickness of the film on the fiber sidewall is a decisive factor in the LOF device performance. The thinnest possible film means that the largest possible number of free volumes or cavities contained in the polymer is able to participate in DNT molecule trapping, enabling a fast response to the presence of the explosive. Moreover, as described in Fig. 1, very thin film makes these cavities fully open to air, which facilitates the cleaning of the trapped analytes with purge gas after measurements are taken, leaving the device ready for its next use. A thick film will offer a stronger initial fluorescent signal. However, because of the greater thickness, some cavities might exhibit greater depths while some other cavities remain either partially or completely hidden under the surface layer of the film. As a result, the analyte trapping process is slow as is the quenching process. Another obvious side effect is that it becomes difficult to remove the analytes trapped by these cavities because they are deeper inside the film.

Unlike the spin-coating process that can control the film thickness by regulating the coater spinning speed, dipping process relies on varying the concentration of the polymer solution to optimize the film thickness. For PL 4a, we prepared four solutions with mass concentrations of 0.02%, 0.03%, 0.07%, and 0.13%. Responses of the LOFs with thin films formed by these solutions are illustrated in Fig. 5. The fluorescent intensities are recorded after 10, 20, and 30 s exposures to the DNT vapor.

Fig. 5 is a perfect example demonstrating the significant influence of the polymer concentration and, thus, the film thickness on the quenching response. For example, within 10 s, the thin film formed from both 0.02% and 0.03% concentration solutions leads to a 30% signal drop. For the 0.13% solution, however, this figure falls to 16%. For a longer exposure such as 30 s, the corresponding signal drops for these three solutions are 87%, 68%, and 47%, indicating that the lower concentration, or thinner film, leads to a faster response. The lowest concentration, however, is limited by the ability of the fluorescent signal detecting system. This becomes more evident in the development of a portable system employing a miniaturized detector whose performance is not comparable with that of lab-based analytical level equipment. In our experiment, an Ocean Optics USB 2000 palm-held spectrometer is used, which requires a longer integration time in order to boost the weak fluorescent signal to an acceptable level. In Fig. 5, for example, a long integration time of 8 s is required for film made from 0.02% concentration solution, whose spectrum shows a strong noise background. A much shorter integration time of 5 s is sufficient for 0.03% concentration but the signal quality is significantly improved. While other higher concentrations show even better signal quality with shorter integration times, 0.03% concentration is deemed to be the best trade-off.

E. Effect of Ambient Light on the Fluorescent Quenching Performance

Degradation of the polymer film when exposed to ambient light resulting in a reduced quenching percentage is an issue that one must be aware of, although fortunately the LOF device always remains in its sealed adaptor module (see Fig. 1) during operation. For a film formed by 0.03% PL 4a solution, we recorded this degradation effect at 0.5 and 12 h after the completion of film formation. The results shown in Fig. 6 clearly demonstrate that after 12 h of ambient light exposure, the film degradation is so significant that the quenching percentages recorded at 10, 20, and 30 s drop to half the level associated with 0.5 h exposure. This is a critical information since the effect of ambient light is easily ignored in the film preparation stage.

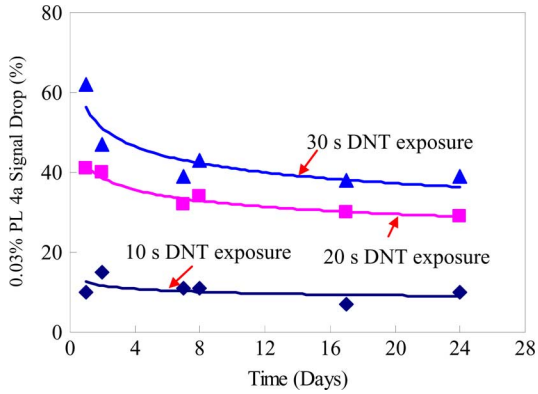

Fig. 7. Evaluation of storage life of PL 4a film over 24 d time following exposure to air containing oxygen but with no ambient light influence. Degradation effect is observable but much less than the ambient light effect in Fig. 6.

F. Storage Life Evaluation of the Polymer Sensory Film

The oxygen contained in the air can also cause degradation of the polymer sensory film. We examined the long-term storage life of these polymers when subject to oxygen alone. The approach we adopted was to make several s-fibers as in Fig. 1 with identical film thickness at the same time in the same solution. They were immediately sealed in a box away from the influence of ambient light after the dipping process. We evaluated the quenching of the film randomly for the next 30 d by simply combining one s-fiber sample with an e-fiber as in Fig. 1 to form an LOF device. Fig. 7 gives the results for the film from 0.03% PL 4a solution for a 24 d time span. Some degradation of the film in terms of reduced quenching percentages indeed occurs over this period but the process is more gradual than with the ambient light effect described in Fig. 6. A much longer life span is expected in reality if some other gas such as nitrogen is used to fill the space containing the LOF device, for example, the adaptor module in Fig. 1.

IV. Conclusion

The critical role of LOFs in the sensor category cannot be overstated in terms of the variety of downsized functional elements on a fiber substrate only a few millimeters long. This paper emphasizes the significance of LOF devices by illustrating their excellent compatibility with the preconcentration unit assisting in the collection of sparse analytes from the open air. Given that any tiny sensor always raises concerns about the system performance, comprehensive evaluation of the LOF device has to be performed. Theoretically we revealed the efficient use of excitation power by this LOF device. Experimentally we extensively examined it by optimizing the thickness and flatness of the sensory thin film, as well as its proper bond to the fiber substrate. The LOF response to the presence of DNT vapor proved to be much faster than the response of the thin film on a bulky planar substrate for all sensory polymers. The degradation of the film due to continuous ambient light illumination and to the oxygen contained in the air was explored as well. In our future study, a particular attention will be given to the adaptor module shown in Fig. 1 since it might overcome these limitations and other potential challenges by conveniently adding additional functionalities. For example, while unexplored in this paper, moisture variation might affect the sensor response and storage life of the polymer. One possible solution could be a moisture control component integrated with the adaptor module. Furthermore, the LOF device and the adaptor module could be packaged together as one compact assembly with the nitrogen gas sealed into its internal airtight chamber that accommodates the LOF device. Such an assembly significantly prolongs both the storage and service life of the sensory polymer since the LOF device-oxygen contact is eliminated once the packaging process is completed. Our further study also includes the effects of the film flatness and thickness associated with the polymer concentrations on the LOF device response. Finally, we will combine this LOF device with a preconcentration unit to detect the presence of TNT explosives in the open air.

References

[1] J. Ma, A. Kos, W. J. Bock, X. Li, H. Nguyen, Z. Y. Wang, and A. Cusano, "Lab-on-a-fiber: Building a fiber-optic sensing platform for low-cost and high-performance trace vapor TNT detection," in *Proc. Int. Soc. Opt. Eng./ 4th Eur. Workshop Opt. Fiber Sens.*, 2010, vol. 7653, pp. 76531E-1–76531E-4.

[2] J. Ma, A. Kos, W. J. Bock, X. Li, H. Nguyen, Z. Y. Wang, and A. Cusano, "TNT vapor detection based on a Lab-on-a-fiber: Achieving a millimeter-scale sensing element on fiber," *IEEE Sens. J.*, vol. 12, pp. 213–217, 2012.

[3] J. Ma, A. Kos, W. J. Bock, X. Li, H. Nguyen, Z. Y. Wang, and A. Cusano, "Enabling low-cost, high-performance vapor-phase TNT detection by optimizing multimode fiber sensing platform," in *Proc. Int. Soc. Opt. Eng./ 21st Int. Conf. Opt. Fiber Sens.*, 2011, vol. 7753, pp. 77535M-1–76535M-4.

[4] H. H. Nguyen, X. Z. Li, N. Wang, Z. Y. Wang, J. Ma, W. J. Bock, and D. Ma, "Fiber-optic detection of explosives using readily available fluorescent polymers," *Macromolecules*, vol. 42, pp. 921–926, 2009.

[5] L. C. Shriver-Lake, K. A. Breslin, P. T. Charles, D. W. Conrad, J. P. Golden, and F. S. Ligler, "Detection of TNT in water using an evanescent wave fiber optic biosensor," *Anal. Chem.*, vol. 67, pp. 2431–2435, 1995.

[6] R. Orghici, U. Willer, M. Gierszewska, S. R. Waldvogel, and W. Schade, "Fiber-optic evanescent field sensor for detection of explosives and CO2 dissolved in water," *Appl. Phys. B: Lasers Opt.*, vol. 90, pp. 355–360, 2008.

[7] J. Ma and W. J. Bock, "Reshaping a sample fluid droplet: Toward combined performance enhancement of an evanescent-wave fiber-optic fluorometer," *Opt. Lett.*, vol. 32, pp. 8–10, 2007.

[8] J. Ma, W. J. Bock, and A. Cusano, "Insights into tunnelling rays: Outperforming guided rays in fiber-optic sensing device," *Opt. Exp.* vol. 17, pp. 7630–7639, 2009.

Author biographies not included at authors' request due to space constraints.